International Journal of Power Electronics and Drive Systems (IJPEDS)
Vol. 12, No. 3, September 2021, pp. 1862~1871
ISSN: 2088-8694, DOI: 10.11591/ijpeds.v12.i3.pp1862-1871

Primary frequency control of large-scale PV-connected multi-machine power system using battery energy storage system

S. M. Imrat Rahman, Md. Rifat Hazari, Sumaiya Umme Hani, Bishwajit Banik Pathik, Mohammad Abdul Mannan, Asif Mahfuz, Mohammad Khurshed Alam, Md. Kamrul Hassan
Department of Electrical and Electronics Engineering, American International University-Bangladesh (AIUB), Dhaka, Bangladesh

Article Info

Article history:

Received Jun 15, 2021
Revised Jul 12, 2021
Accepted Jul 23, 2021

Keywords:

Battery energy storage system
Droop control
Frequency oscillation
Power system
PV System

ABSTRACT

Large-scale grid-tied photovoltaic (PV) station are increasing rapidly. However, this large penetration of PV system creates frequency fluctuation in the grid due to the intermittency of solar irradiance. Therefore, in this paper, a robust droop control mechanism of the battery energy storage system (BESS) is developed in order to damp the frequency fluctuation of the multi-machine grid system due to variable active power injected from the PV panel. The proposed droop control strategy incorporates frequency error signal and dead-band for effective minimization of frequency fluctuation. The BESS system is used to consume/inject an effective amount of active power based upon the frequency oscillation of the grid system. The simulation analysis is carried out using PSCAD/EMTDC software to prove the effectiveness of the proposed droop control-based BESS system. The simulation result implies that the proposed scheme can efficiently curtail the frequency oscillation.

Corresponding Author:

S. M. Imrat Rahman
Department of Electrical and Electronics Engineering
American International University-Bangladesh (AIUB)
408/1, Kuratoli, Khilkhet, Dhaka 1229, Bangladesh
Email: imratrahman@aiub.edu

1. INTRODUCTION

In the 21st century, renewable energy-based power sources integration to the central power network has risen sharply due to the increased need for electrical energy [1]. Moreover, harnessing clean energy from renewable technologies has significantly reduced carbon emissions and air pollution [2]. In recent times, among all other renewable resources, solar has achieved its own prominent position and it is estimated that 70% of the global energy will be produced employing solar technology by the year of 2100 [3]. In 2019, the global installed solar capacity was 586.434 GW, of which 580.15 GW was solar PV [4]. Solar PV systems have seen an exponential growth rate in recent years, and in 2019 alone, approximately 100 GW of PV capacity was added all over the world [5].

Since the output from PV systems will vary depending on weather conditions, there will be a considerable influence on the electrical grid. Again, the grid frequency greatly varies with the real power balance [6]. As solar energy is intermittent in nature, there will be an imbalance in power between the generation side and load side. Therefore, the system frequency will fluctuate, and it will affect power system performance, reliability, and efficiency [6]. Immense fluctuation in the grid frequency is the repercussion of incorporating solar PV systems in large scale to the electric grid.

In some literature, some techniques are used to minimize frequency oscillation due to PV system. For example, in [7]-[10], the PV system is operated in deloading mode. However, active power reservation due to deloading operation will reduce the injected power from the PV panel. In [11], the oversize DC-Link capacitor is used as energy buffer, but it has small delivery time. Super magnetic energy storage (SMES) [12] and electric double layer capacitor (EDLC) [13] are also used to minimize frequency oscillation. However, the SMES and EDLC can be applied only up to few MW scale [14]. On the other hand, integration of BESS can help to mitigate frequency oscillation problems in large-scale grid-tied PV system.

Therefore, the key contributions of this paper are: (i) An appropriate droop control technique of BESS is designed with the aim of diminishing the frequency variation. The proposed frequency dependent droop controller of BESS is composed of frequency error signal, droop gain and dead-band to ensure effective use of BESS active power. This is the prominent aspect of this study. (ii) The resilient performance of the developed droop-controlled BESS system is explored using simulation evaluations on a multi-machine IEEE nine-bus system model that includes a PV system and conventional power plants. (iii) This paper also portrays the detail explanations of PV module, PV control systems, IEEE nine-bus power system, PV power plants along with its control mechanism as well as proposed BESS.

The remaining sections of the paper are organized as follows: Section 2 describes the system model; Section 3 and 4 explains the PV power plant and proposed BESS control method, respectively. The simulation results and discussion are offered in Section 5 and lastly the conclusion has been drawn in Section 6 with the future recommendation.

2. POWER SYSTEM MODEL

Figure 1 demonstrates the system model which is comprised of a nine-bus main system [15] together with a PV plant and a BESS. Three conventional power plants are present in the main nine bus system. synchronous generator 1 (SG1) and SG2 represent two thermal power plants with ratings of 150 MVA and 250 MVA respectively. SG3 represents a hydro power plant with a rating of 200 MVA. Automatic generation control (AGC) is applied for operating both SG1 and SG3 while governor-free (GF) control is applied for SG2. The parameters of the SGs are based on [16]. For all the conventional SGs, the IEEE type AC4A excitation system presented in Figure 2 (a) has been considered [17]. The reheat steam turbine governor model [17] presented in Figure 2 (b) is used for the steam power plants (SG1 and SG2). Figure 2 (c) illustrates the hydro turbine governor model [17] employed for hydro power plant. Typical values of the turbine parameters are based on [17]. Figure 2 (d) shows the integral controller which has been included for AGC operation in the governor systems [17]. Here integral gain *Ki* is fixed at 6.

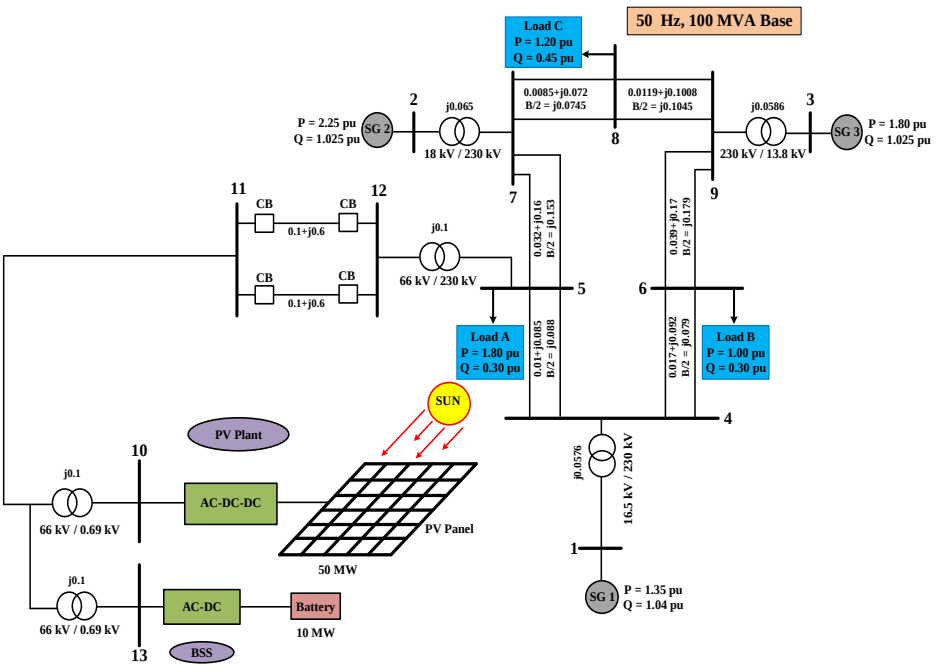

Figure 1. Power system model

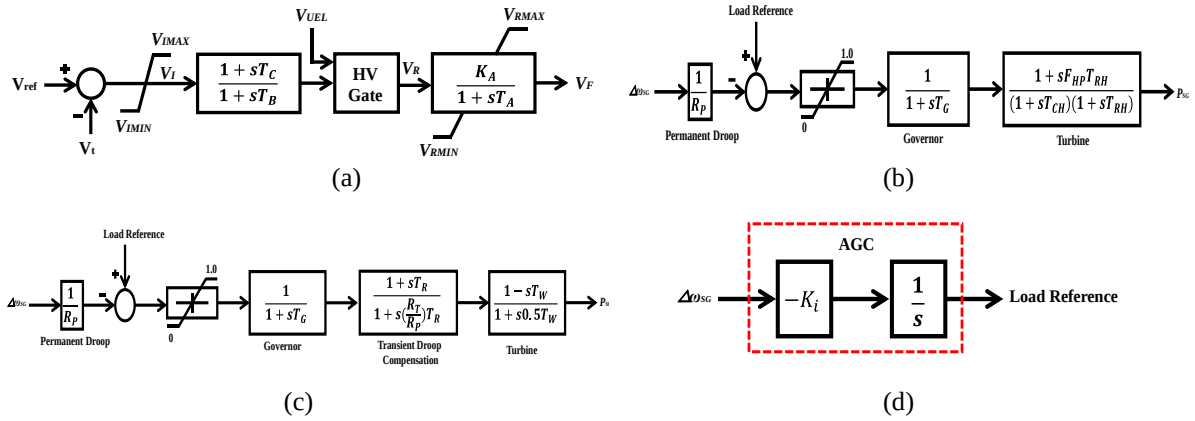

Figure 2. Components of synchronous generator, (a) IEEE type AC4A exciter, (b) Governor system of steam turbine, (c) Governor system of hydro turbine, (d) Integral controller

A PV system and BESS are attached to the Bus 5 of the main IEEE nine bus system using dual transmission lines. The capacity of PV system and BESS are 50 MW and 10 MW, respectively.

3. PV SYSTEM MODEL

3.1. PV module design

Figure 3 delineates the equivalent circuit of a single solar cell employing single diode model [18]. The equivalent circuit applied in this work has a current source, single diode and parallel and series resistors. The expression for resultant current of a single solar cell is as follows [18-21]:

$$I = I_{PV} - I_o \left[exp\left(\frac{V+R_s I}{aV_t}\right) - 1 \right] - \frac{V+R_s I}{R_p} \quad (1)$$

Here, I_{PV} is the photo current which is produced after exposing the solar cell to solar irradiation and I_o is the reverse saturation current of diode. Diode identity factor is expressed with a. R_s and R_p are the resistances in series and parallel, respectively. V_t is the thermal voltage, where N_s represents number of series connected PV cells, T is the cell temperature, q is the electron charge and k is the Boltzmann constant.

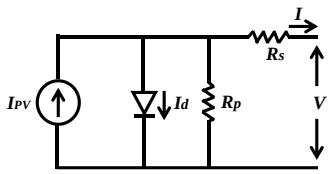

Figure 3. Equivalent circuit of solar cell

I_{PV} will fluctuate depending on the temperature and solar irradiation and it can be noticed through the (2):

$$I_{PV} = \left(I_{pv}, n + K_I \Delta T\right) \frac{G}{G_n} \quad (2)$$

Here, I_{pv},n represents photocurrent under normal condition (temperature is 25^{o}C and solar irradiation is 1000 W/m^2), K_I indicates the short circuit current per temperature coefficient, G and G_n represents solar surface irradiation of the module and solar irradiation during nominal situation respectively, and ΔT is the difference between G and G_n [19]. The equations for I_{pv},n and I_o are as follows [21]:

$$I_{PV,n} = \frac{R_p + R_s}{R_p} I_{sc,n} \quad (3)$$

$$I_{sc} = \frac{I_{sc,n}+K_I\Delta T}{exp\left(\frac{V_{oc,n}+K_V\Delta T}{aV_t}\right)-1} \quad (4)$$

Here, $V_{oc,n}$ and $I_{sc,n}$ are the open circuit voltage and short circuit current, respectively under nominal conditions. K_V represents the open circuit voltage per temperature coefficient. In this work, solar module of Kyocera KC200GT is utilized to design the PV system [22]. The expression for a PV power plant with numerous solar modules is as [18], [23], [24]:

$$I = N_P I_{PV} - N_P I_o \left[exp\left(\frac{(V+R_S\left(\frac{N_M}{N_P}\right)I}{N_M a V_t}\right) - 1\right] - \frac{V+R_S\left(\frac{N_M}{N_P}\right)I}{R_p\left(\frac{N_M}{N_P}\right)} \quad (5)$$

Here, N_M and N_P are the number of modules connected in series in a string and the number of parallel strings, respectively. The I-V and P-V characteristics of the PV plant is illustrated in Figure 4.

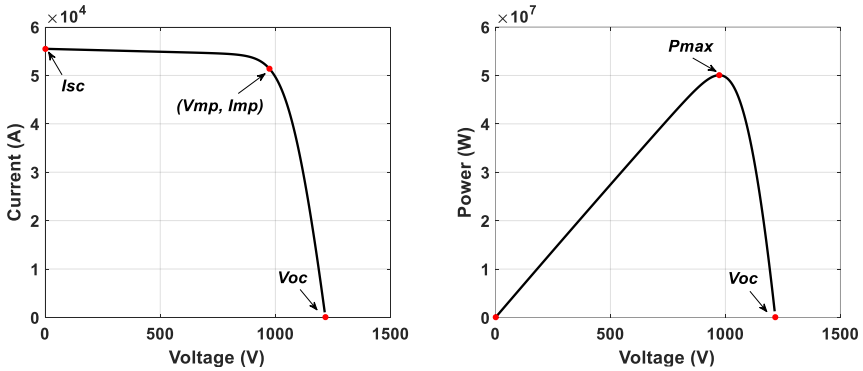

Figure 4. Characteristics curves of a 50 MW PV power plant, (a) I-V curve, (b) P-V curve

3.2 Control method of PV system

The PV plant together with the designed control scheme is presented in Figure 5. The PV system is comprised of 50 MW PV module, boost converter for DC/DC conversion and inverter from DC/AC conversion. The controller for boost converter operates the DC/DC converter and controller for grid side inverter operates the DC/AC converter. The gate signals for the insulated gate bipolar transistors (IGBTs)-based converters are generated using pulse width modulation (PWM) technique. The DC line used in this study is based on [25]. In order to acquire maximum power available from the plant, the DC/DC boost converter regulates the voltage obtained from the plant. For this purpose, fractional open circuit voltage-based algorithm has been applied for extracting maximum amount of power. The relationship between voltage at maximum power (V_{mp}) and open circuit voltage (V_{OC}) can be expressed as follows:

$$V_{mp} = K_{mp}V_{oc} \quad (6)$$

Here, K_{mp} is a proportional constant with a value of 0.8023 for solar module of KC200GT [22]. Reference duty cycle can be generated using (7):

$$D_{ref} = 1 - \frac{N_M K_{mp} V_{oc\_pilot}}{V_o} \quad (7)$$

Here, V_o is the boost converter output voltage and V_{oc_pilot} represents module voltage at open circuit condition

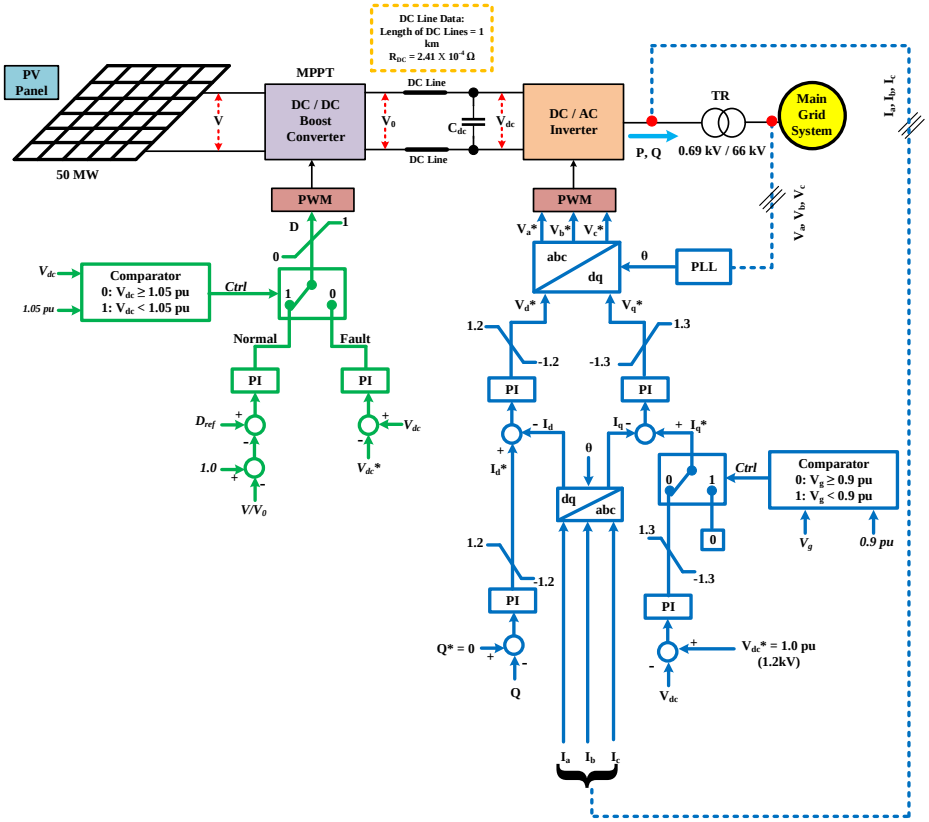

Figure 5. PV system configuration

With the occurrence of any grid fault, the PV panel's DC power cannot be fed to the network because of voltage drop. As a result, the DC-link voltage rises dramatically. To solve this issue, an extra control scheme shown in Figure 5 has been included in the boost converter controller, which bypasses the maximum power point tracking (MPPT) controller for severe grid fault. The inclusion of this additional control scheme allows the DC-link voltage to remain in the range. The four PI controllers make the DC/AC converter as presented in Figure 5. The reactive power distributed to the grid is regulated by a grid side inverter controller. Additionally, the DC-link voltage is kept steady by this controller. The reference of reactive power is fixed to 0.0 pu. During fault condition, the comparator ensures that no active power is distributed to the grid.

4. PROPOSED BESS AND DROOP CONTROL STRATEGY

The proposed BESS with droop control scheme is depicted in Figure 6. The BESS model consists of DC voltage source, PWM based voltage source inverter (VSC) and a step-up transformer. The VSC converts DC voltage into three phase AC voltage with grid frequency. The proposed control technique is illustrated in the bottom part of Figure 6. Here, four PI controllers have been utilized to compensate the error signals. The real power sent to the grid is controlled by regulating the current of d-axis (I_d) and the reactive power exerted to the grid is controlled by regulating current of q-axis (I_q).

The frequency of the grid is stabilized by the droop controller which receives power system frequency (f) as feedback. Subsequently, frequency fluctuation is reduced by delivering/consuming appropriate amount of active power from the BESS. A dead-band in the scheme ensures that the droop controller is operated only when the frequency fluctuation is outside of a specific range. The droop gain (K_{droop}) is chosen such that optimum results are obtained. Hence, the reference active power (P^*) will be:

$$P^*=K_{droop}\Delta f \quad (8)$$

To ensure unity power factor, the reference reactive power is fixed to 0.0 pu. The outer loop PI controller will compensate for the error signal between the actual and the reference reactive power. Finally,

the gate drive pulses are generated by comparing the reference voltages with a triangular carrier wave that has a high frequency. In this way, the designed droop controller can minimize frequency fluctuations.

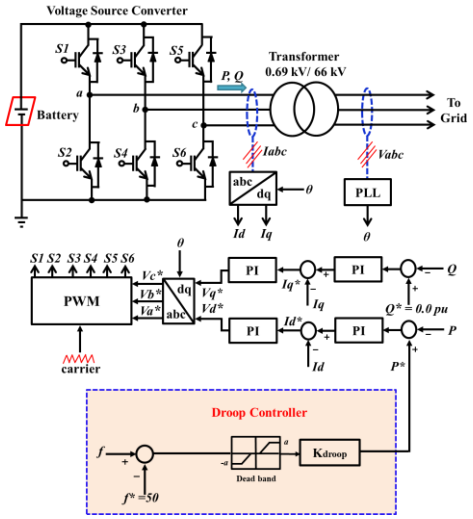

Figure 6. Proposed BESS with droop control strategy

5. SIMULATION RESULTS AND DISCUSSION

5.1. Analysis of steady-state condition

In this work, the power system model demonstrated in Figure 1 is used for simulation analysis. PSCAD/EMTDC software has been used for performing the analysis on the following two cases:

Case 1: Without BESS

Case 2: With the proposed droop-controlled BESS

The solar irradiance data used for the analysis and the active power output from the PV system is presented in Figures 7 (a) and 7 (b) respectively. Extreme cases of variation in solar irradiance have been considered for analyzing the performance of the proposed scheme.

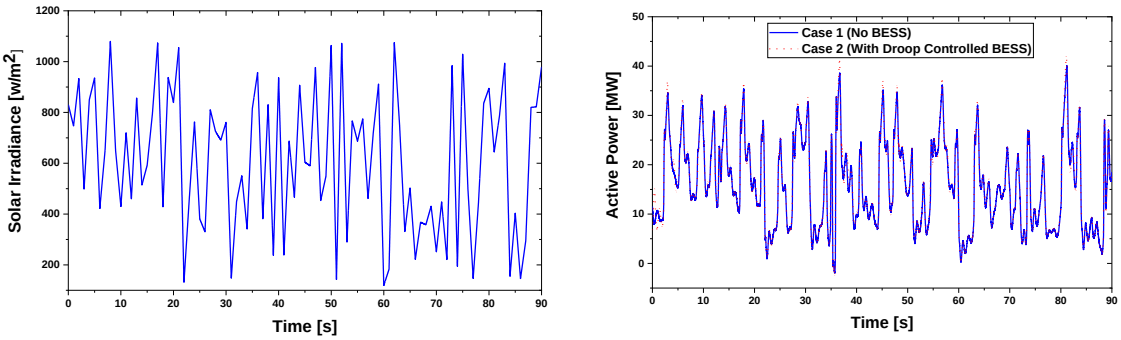

(a) (b)

Figure 7. Input solar irradiance and output active power of the PV system, (a) applied solar irradiance, (b) output of active power of PV system

The active power output from a PV system varies according to the amount of solar irradiance as presented in Figure 7 (b). It can be observed that there are negligible changes in active power between the two cases as the PV plant is feeding power to the grid directly, and the same control method has been applied to the PV system. The frequency response of the system is presented in Figure 8 (a). It can be noticed that the frequency fluctuation is very high for Case 1 due to the variation of active power injected into the grid from PV system. On the other hand, after incorporating the proposed BESS controlled by droop controller into the terminal of PV system, there has been a drastic reduction in frequency fluctuation in Case 2, as shown in

Figure 8 (a). This is because the BESS is regulating the frequency by providing/absorbing active power, as presented in Figure 8 (b) from the grid in Case 2. The integrated dead band control allows the droop controller to be operated only when the fluctuation has surpassed a certain threshold. In case of reduction in system frequency from the nominal value, the BESS is providing real power. Alternatively, with increased frequency, the BESS absorbs the real power from the grid in Case 2.

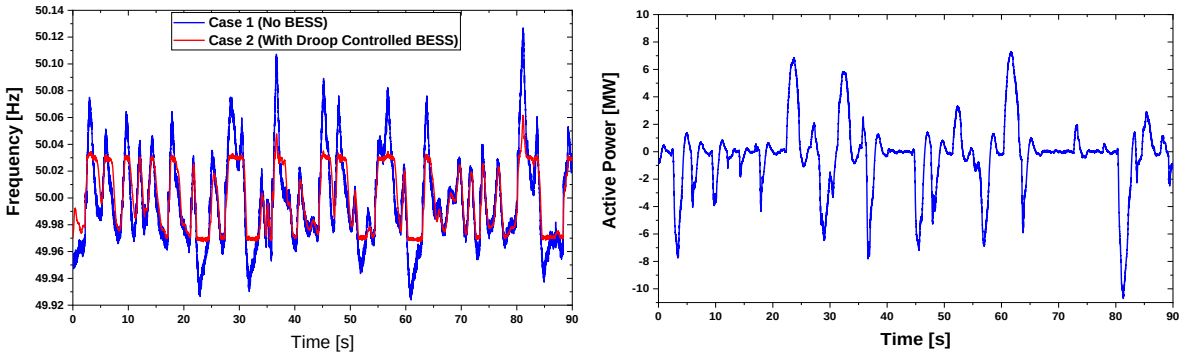

(a) (b)

Figure 8. Frequency response and active power output of BESS, (a) power system frequency response, (b) output of active power of BESS (case 2)

Finally, Figure 9 illustrates the active power outputs from the conventional generators. Without BESS system, the SGs outputs are fluctuating higher as they are compensating the variation in active power generated by the PV system taking all the loads into account. By adopting the proposed droop controller, the power output from the SGs is fluctuating less since the compensation is carried out by the BESS now.

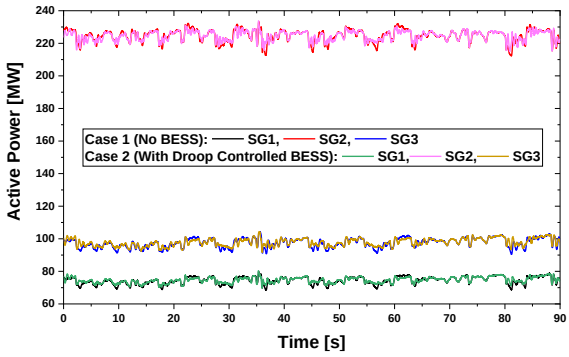

Figure 9. Output of active power of conventional power plants

Table 1 shows the maximum frequency deviation along with the standard deviation for Case 1 and Case 2. It can be seen from Table 1 that $+\Delta f$, $-\Delta f$, and σ are lesser for Case 2. Following the implementation of the proposed BESS, 30% reduction in the standard deviation of the frequency fluctuation was observed. So, it can be verily acknowledged that the proposed droop controller-based BESS can provide adequate primary frequency control.

Table 1. Comparison of parameters from frequency response graph under steady-state condition

Frequency parameters	Case 1	Case 2
Highest frequency variation in positive direction ($+\Delta f$)	0.12691	0.06171
Lowest frequency variation in negative direction ($-\Delta f$)	-0.07609	-0.03262
Standard deviation (σ)	0.0337	0.0236

5.2. Analysis of load variation

In this analysis, the same power system model presented in Figure 1 is used. However, load B has been increased to 160 MW at 10 s and reduced to 60 MW at 20 s to validate the effectiveness of the proposed BESS system during overload and underload events. The irradiance applied to PV system is presented in Figure 10 (a). Figure 10 (b) illustrates the frequency response. It is observed that the frequency can be well controlled both in overload and underload events in Case 2, whereas considerable fluctuation has occurred in Case 1. The frequency response in Case 2 is more stable because of injecting power during overload and consuming power during underload events from the BESS as presented in Figure 10 (c). Additionally, $+\Delta f$, $-\Delta f$, and σ computed from Figure 10 (b) is smaller in proposed Case 2 than in Case 1, as depicted in Table 2. Thus, it is possible to infer that both in overload and underload scenarios, the suggested BESS system regulates the system frequency properly.

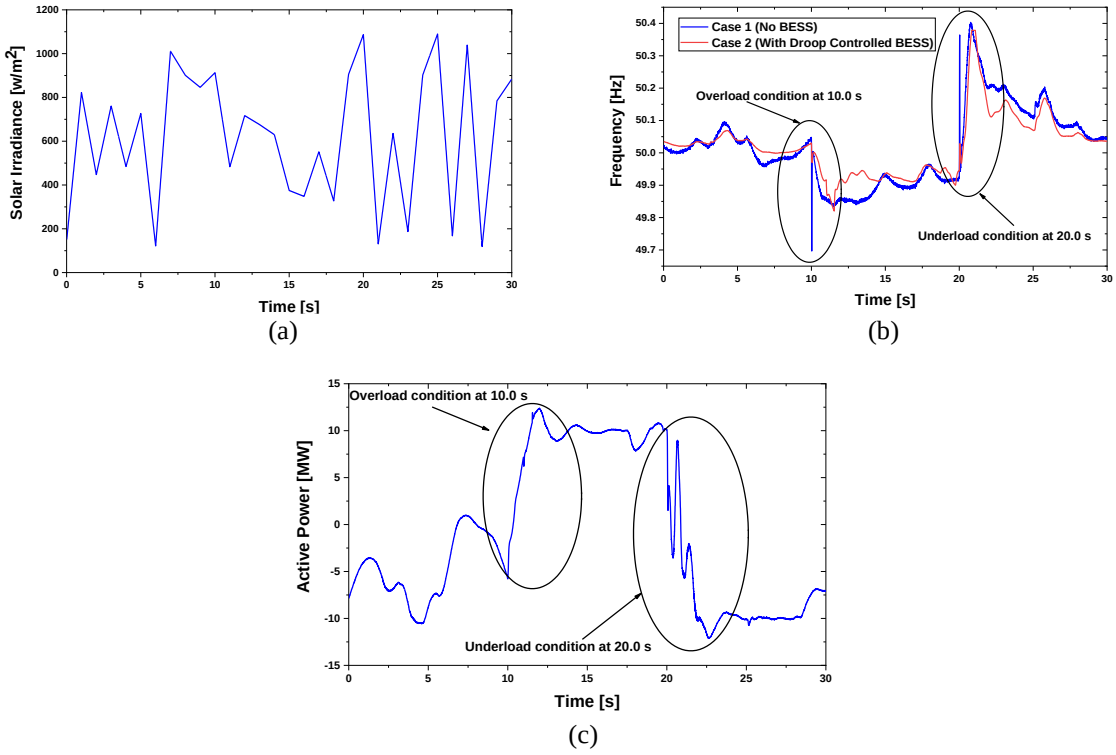

Figure 10. Various responses of the power system under load variation
(a) applied solar irradiance, (b) power system frequency, (c) active power of BESS (Case 2)

Table 2. Comparison of parameters from frequency response graph under load variation

Frequency parameters	Case 1	Case 2
$+\Delta f$	0.4034	0.3785
$-\Delta f$	-0.3033	-0.1800
σ	0.1176	0.0914

5.3. Analysis of fault condition

In this analysis, a three-line-to-ground (3LG) fault has been applied on one of the transmission lines near bus 11 of the power system model presented in Figure 1. The fault conditions are presented in Figure 11. The simulation period is 10.0 s. The fluctuating solar irradiance applied in this fault analysis, is given in Figure 12 (a). The frequency of the power system is more stable after the 3LG fault, as shown in Figure 12 (b). This is because the BESS injects/consumes reactive power based on the frequency deviation, as shown in Figure 12 (c). The effectiveness of the proposed BESS system is also clearly seen in Table 3. All the variations are more diminutive in Case 2 than in Case 1.

Figure 11. Condition of 3LG fault

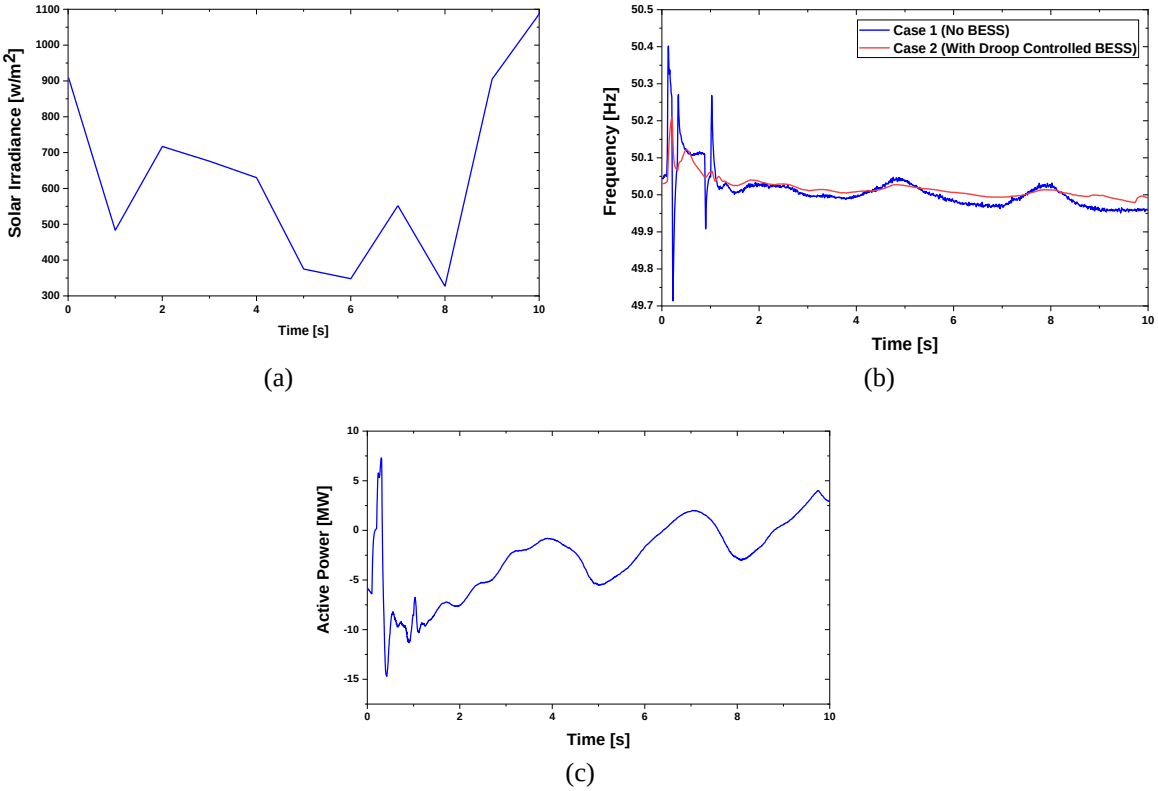

Figure 12. Various responses of the power system under fault condition: (a) applied solar irradiance, (b) power system frequency, (c) active power of BESS (Case 2)

Table 3. Comparison of parameters from frequency response graph under 3LG fault

Frequency parameters	Case 1	Case 2
$+\Delta f$	0.4019	0.2099
$-\Delta f$	-0.2864	-0.0206
σ	0.0529	0.0292

6. CONCLUSION

A novel control framework based on BESS and droop control has been proposed in this work for primary frequency control of large-scale PV-connected multi-machine systems. The addition of a dead-band control ensures the droop controller will operate only when the frequency fluctuation has exceeded a certain threshold value. The comprehensive design technique of the proposed BESS and the control scheme have also been presented in this work. The proposed BESS can stabilize the grid frequency by adjusting the active power delivered and absorbed from the electric grid. The performance of the proposed control model has been tested by applying a wide range of solar irradiance data with rapid variations, underload, overload, and fault conditions. Simulation results show that maximum frequency deviation has been reduced drastically after the application of the proposed BESS. Thus, the proposed control scheme can significantly minimize the frequency variation and stabilize the grid for a large-scale PV-connected system.

REFERENCES

[1] H. Bevrani, A. Ghosh, and G. Ledwich, "Renewable energy sources and frequency regulation: survey and new perspectives," *IET Renewable Power Generation*, vol. 4, no. 5, pp. 438-457, 2010, doi: 10.1049/iet-rpg.2009.0049.

[2] A. H. M. S. Ula, "Global warming and electric power generation: What is the connection?," in *IEEE Transactions on Energy Conversion*, vol. 6, no. 4, pp. 599-604, Dec. 1991, doi: 10.1109/60.103631.

[3] "World energy resources: solar world energy council," 2013. [Online]. Available: https://www.worldenergy.org/assets/images/impor ted/2013/09/Complete_WER_2013_Survey.pdf

[4] IRENA, Renewable capacity statistics 2020 International Renewable Energy Agency IRENA, Abu Dhabi.

[5] Photovoltaic power systems programme annual report, 2019. Available: https://iea-pvps.org/wp-content/uploads/2020/05/IEA-PVPS-AR-2019-1.pdf.

[6] H. Bevrani, "*Robust Power System Frequency Control*," USA, NY, New York: Springer, 2009.

[7] E. I. Batzelis, G. E. Kampitsis, and S. A. Papathanassiou, "Power reserves control for PV systems with real-time MPP estimation via curve fitting," in *IEEE Transactions on Sustainable Energy*, vol. 8, no. 3, pp. 1269-1280, July 2017, doi: 10.1109/TSTE.2017.2674693.

[8] H. Xin, Y. Liu, Z. Wang, D. Gan, and T. Yang, "A new frequency regulation strategy for photovoltaic systems without energy storage," in *IEEE Transactions on Sustainable Energy*, vol. 4, no. 4, pp. 985-993, Oct. 2013, doi: 10.1109/TSTE.2013.2261567.

[9] A. F. Hoke, M. Shirazi, S. Chakraborty, E. Muljadi, and D. Maksimovic, "Rapid active power control of photovoltaic systems for grid frequency support," in *IEEE Journal of Emerging and Selected Topics in Power Electronics*, vol. 5, no. 3, pp. 1154-1163, Sept. 2017, doi: 10.1109/JESTPE.2017.2669299.

[10] S. I. Nanou, A. G. Papakonstantinou, and S. A. Papathanassiou, "A generic model of two-stage grid-connected PV systems with primary frequency response and inertia emulation," *Electric Power Systems Research*, vol. 127, pp. 186–196, 2015, doi: 10.1016/j.epsr.2015.06.011.

[11] J. Fang, H. Li, Y. Tang, and F. Blaabjerg, "Distributed power system virtual inertia implemented by grid-connected power converters," in *IEEE Transactions on Power Electronic*s, vol. 33, no. 10, pp. 8488-8499, Oct. 2018, doi: 10.1109/TPEL.2017.2785218.

[12] H. -Y. Jung *et al*., "A study on the operating characteristics of SMES for the dispersed power generation system," in *IEEE Transactions on Applied Superconductivity*, vol. 19, no. 3, pp. 2028-2031, June 2009, doi: 10.1109/TASC.2009.2018495.

[13] N. Kakimoto, H. Satoh, S. Takayama, and K. Nakamura, "Ramp-rate control of photovoltaic generator with electric double-layer capacitor," in *IEEE Transactions on Energy Conversion*, vol. 24, no. 2, pp. 465-473, June 2009, doi: 10.1109/TEC.2008.2001580.

[14] S. Shivashankar, S. Mekhilef, H. Mokhlis, and M. Karimi, "Mitigating methods of power fluctuation of photovoltaic (PV) sources – A review," *Renewable and Sustainable Energy Reviews*, vol. 59, pp. 1170–1184, 2016, doi: 10.1016/j.rser.2016.01.059.

[15] P. P. Anderson, and A. A. Fouad, *Power system control & stability*, John Wiley & Sons: Oxford, UK, 2008.

[16] M. Hazari, M. Mannan, S. Muyeen, A. Umemura, R. Takahashi, and J. Tamura, "Stability augmentation of a grid-connected wind farm by fuzzy-logic-controlled DFIG-based wind turbines," *Applied Sciences*, vol. 8, no. 1, p. 20, pp. 1-24, Dec. 2017, doi: 10.3390/app8010020.

[17] P. Kundur, *Power system stability & control*, McGraw-Hill Inc.: New York, NY, USA.

[18] H. M. Hasanien, "An adaptive control strategy for low voltage ride through capability enhancement of grid-connected photovoltaic power plants," in *IEEE Transactions on Power Systems*, vol. 31, no. 4, pp. 3230-3237, July 2016, doi: 10.1109/TPWRS.2015.2466618.

[19] H. M. Hasanien, "Shuffled frog leaping algorithm for photovoltaic model identification," in *IEEE Transactions on Sustainable Energy*, vol. 6, no. 2, pp. 509-515, April 2015, doi: 10.1109/TSTE.2015.2389858.

[20] Y. A. Mahmoud, W. Xiao, and H. H. Zeineldin, "A Parameterization approach for enhancing PV model accuracy," in *IEEE Transactions on Industrial Electronics*, vol. 60, no. 12, pp. 5708-5716, Dec. 2013, doi: 10.1109/TIE.2012.2230606.

[21] R. Kadri, J. Gaubert, and G. Champenois, "An improved maximum power point tracking for photovoltaic grid-connected inverter based on voltage-oriented control," in *IEEE Transactions on Industrial Electronics*, vol. 58, no. 1, pp. 66-75, Jan. 2011, doi: 10.1109/TIE.2010.2044733.

[22] G. M. S. Islam, A. Al-Durra, S. M. Muyeen, and J. Tamura, "A robust control scheme to enhance the stability of a grid-connected large scale photovoltaic system," *PES T&D 2012*, 2012, pp. 1-6, doi: 10.1109/TDC.2012.6281420.

[23] M. K. Hossain, and M. H. Ali, "Low voltage ride through capability enhancement of grid connected PV system by SDBR," *2014 IEEE PES T&D Conference and Exposition*, 2014, pp. 1-5, doi: 10.1109/TDC.2014.6863248.

[24] M. R. Starke, "DC distribution with fuel cells as distributed energy resources," Ph.D. dissertation, Dept. Electric. Eng., Univ. Tennessee, Knoxville, 2009.

[25] S. M. Istiaque Mahmud, M. A. Mannan, and M. R. Hazari, "LVRT performance analysis and transient stability augmentation of a grid-tied PV system," *2021 2nd International Conference on Robotics, Electrical and Signal Processing Techniques (ICREST)*, 2021, pp. 48-52, doi: 10.1109/ICREST51555.2021.9331231.